International Journal of Sustainable Development and Planning
Vol. 20, No. 12, December, 2025, pp. 5043-5057
Journal homepage: http://iieta.org/journals/ijsdp

From Palm Groves to Urban Zones: Patterns and Past Trends of Urban Sprawl and Land Use Efficiency in Semi-Arid Context, Case of Biskra, Algeria

Fouad Leghrib[1*], Said Mazouz[2], Federico Martellozzo[3]

[1] LACOMOFA Laboratory, Department of Architecture, Faculty of Architecture, Urbanism, Civil-Engineering and Hydraulics, University of Biskra, Biskra 07000, Algeria
[2] LEQUAREB Laboratory, Department of Architecture, University of Oum El Bouaghi, Oum El Bouaghi 04000, Algeria
[3] Department of Economics and Management, University of Florence, Florence 50121, Italy

Corresponding Author Email: f.leghrib@univ-biskra.dz

https://doi.org/10.18280/ijsdp.201202

Received: 20 November 2025
Revised: 15 December 2025
Accepted: 19 December 2025
Available online: 31 December 2025

Keywords:
Biskra urban area, GIS, land use efficiency, land use land cover change, remote sensing, sustainable development goals, urban sprawl

ABSTRACT

Cities worldwide are experiencing rapid expansion, often leading to urban sprawl that encroaches on adjacent agricultural land. This phenomenon represents a significant challenge for sustainable urban development. In this context, the present study investigates land use efficiency by assessing the spatiotemporal dynamics of urban sprawl in the Biskra urban area, Algeria, over a twenty-year period. Using a retrospective, integrated remote sensing (RS) and GIS approach, multi-temporal Landsat imagery was processed via supervised classification using the maximum likelihood algorithm. Land use land cover changes were further analyzed using post-classification comparison of image pairs spanning two decades to determine the magnitude, direction, and nature of transformations. Findings reveal that prevailing urban policies have contributed to inefficient land management practices, leading to sprawling urban patterns and significant land-use changes. During the first decade of the 2000s, urban expansion accelerated sharply, with the built-up area increasing at a rate nearly four times higher than population growth. As a result, three previously distinct municipalities merged into a single, continuous urban zone, accompanied by extensive conversion of palm groves into built-up areas. By revealing how current planning practices have contributed to unsustainable land-use patterns, the findings highlight the need to align local urban management strategies with broader global sustainability frameworks that align with the objectives of the Sustainable Development Goals (SDGs).

1. INTRODUCTION

For centuries, cities were characterized by their compact form and high population density; they expanded slowly within their ramparts [1]. However, over the last 40 years, this tendency has been reversed. Nowadays, cities worldwide are expanding twice the rate of population growth [2], resulting in unprecedented and irreversible urban sprawl. Hence, advocates for sustainable urban development, planners, and policymakers are devoting greater attention to urban sprawl [3].

Based on the definition of the European Environment Agency (EEA), "Urban sprawl occurs when the growth rate of urbanized areas exceeds the population growth rate" [4]. In the United States, the definition is very similar to that of the EEA, while specifying the dominance of low-density urban areas [5, 6], rapid expansion and random development [7]. On the continuum of anthropogenic actions, urbanization is the primary driver of urban sprawl and land use land cover (LULC) changes, with urban areas expanding onto prime agricultural land and protected areas [8-10]. In addition to urban sprawl, LULC change itself produces other forms of environmental change and often leaves a lasting legacy of impact on the ecological features of a landscape [11-18].

Urban sprawl can strain resources and compromise environmental quality. It presents a significant challenge for cities struggling to balance development with environmental sustainability, particularly in developing countries, where unplanned expansion and inefficient land use threaten their future.

Despite the global advancement of RS and GIS applications for analyzing, monitoring, and modeling urban sprawl and LULC change, these approaches remain insufficiently explored in the Algerian context. This study addresses this gap by examining Land-Use Efficiency (LUE) and the spatiotemporal dynamics of urban sprawl in the Biskra Urban Area over twenty years (2000–2020).

2. LITERATURE REVIEW

2.1 Monitoring urban sprawl through LULC change: A GIS-based approach

Researchers worldwide use LULC change studies to

investigate urban sprawl and better understand land use changes over a known period of time [19]. The outcomes of the studies assist decision-makers in monitoring urban sprawl and implementing land-use policies to meet the rising land demand driven by population growth. Land use/cover terminology is frequently used interchangeably [20]. Land cover represents the characteristics of the earth's surface, including bare soil and vegetation. Whereas land use focuses on the functional role of land for economic activities and the ways that land is used by humans, for example, built-up area and agriculture, etc. [21].

The main drivers of LULC change are natural phenomena and anthropogenic activities associated with human actions [22]. Understanding the interactions among these drivers is crucial for effective land management and improved decision-making. Unfortunately, in developing countries, the assessment of urban sprawl and LULC changes continues to rely on expensive, time-consuming conventional survey methods [14-23]. As a result, researchers are increasingly interested in using Geographic Information Systems (GIS) and remote sensing (RS) techniques to map and monitor urban sprawl [24].

LULC change studies are based on remotely sensed data and GIS techniques, providing an appropriate platform for improved data analysis accuracy at lower cost and in less time. Since then, LULC mapping has become the principal application of RS, particularly after the emergence of higher resolution satellite data and more sophisticated image processing [25, 26]. Nevertheless, detecting LULC changes in the urban context, particularly in arid and semi-arid regions, remains a significant challenge due to the variability and coexistence of urban landscape elements [27]. Various LULC change detection methods are used to analyze past LULC change trends, namely Image Segmentation, object-oriented classification, neural networks, and conventional cross-tabulation. Each of these approaches has its advantages and drawbacks; however, no single technique can fully explain the LULC change-detection problem [28].

2.2 Exploring urban sprawl trends: Insights from developing countries

RS and GIS Integrated approaches have been implemented in countless urban sprawl studies.

For instance, Al-Rashid et al. [10] used a combined method to examine urban sprawl patterns and LULC change from 1990 to 2018 in Sialkot, Pakistan. They compared the results with urban development policies outlined in earlier master plans. The research outcomes revealed that the city is moving towards urban sprawl.

Similarly, Rawat and Kumar [20] conducted a study on LULC changes in the Hawalbagh block, district Almora, India, from 1990 to 2010. They adopted the supervised classification methodology. The study highlighted the importance of satellite images and change-detection methods for quantifying and analyzing of landscape dynamics that traditional mapping procedures cannot accurately represent.

Furthermore, Shikary and Rudra [29] applied a combined geospatial method using Shannon's entropy model to measure urban land-use change and sprawl in Purulia District, India. Supervised classification was applied to investigate urban expansion from 1998 to 2018. The outcomes demonstrate that despite the compact trend of urban expansion in Purulia, urban areas have been progressively shrinking from the CBD to the periphery.

Finally, Chettry and Surawar [30] analyzed urban sprawl in several Indian cities by combining GIS and remote sensing with a multivariable integrated urban sprawl index (USI). The research concluded that, despite a decline in population density in most cities, the analysis highlighted the dominance of outward expansion.

2.3 GIS techniques in urban planning: A review of the Algerian context

In Algeria, most of the literature on the use of GIS and RS techniques to detect and monitor LULC changes is carried out in the fields of biodiversity, ecology, hydrology, forestry, agronomy, and pedology. For example, landslide susceptibility [31-33], water quality [34], desertification sensitivity [35, 36], land degradation and soil salinization [37-39], land suitability [40, 41], erosion sensitivity [42-44], forest fires [45-47], urban green spaces [48], forest cover changes [49], flood risk [50-52].

In the field of urban planning in the Algerian context, scarce literature exists about the topic, as observed in the study carried out by Leghrib et al. [53] on the advantages and drawbacks of urban growth models and LULC change detection techniques and how such tools may be applied in the Algerian urban planning practice. The study concluded that despite their massive use at the international level, the implementation of LULC change detection techniques in the process of urban planning and decision-making in Algeria is still lagging due to several constraints, at the forefront of them the lack of recent data processing equipment, unavailability of relevant and accurate data and the shortage of financial resources and trained personnel.

Bouhata et al. [54] examined urban expansion in Biskra City between 1987 and 2016 using several Landsat satellite images and GIS techniques. Adel et al. [55] applied geomatics tools to detect non-compliance between conventional development plans (master plans) and on-the-ground reality, leading to excessive and uncontrolled urbanization. Nedjai et al. [56] used the Land Change Modeler to assess and forecast LULC changes in Algiers. The predictive scenario for 2030 showed that 80% of the city will be developed and transformed into built-up areas, which supports the upcoming land crisis in Algiers. Dechaicha et al. [57] used landscape metrics and multi-temporal Landsat data to highlight urban growth dynamics in Adrar, Algeria, from 1986 to 2016. The study shows the excessive loss of palm groves and the impact of urbanization on oasis ecosystems. Dridi et al. [58] used remotely sensed data to assess urban sprawl in Batna City between 1972 and 2013. They adopted Support Vector Machine (SVM) and Shannon's Entropy to detect and monitor the urban sprawl phenomenon.

3. MATERIALS AND METHODS

3.1 Study area

Biskra Province (wilaya) is a key city in south-eastern Algeria, situated 400 km from the capital, Algiers (Figure 1). It is divided into 27 municipalities (33 municipalities previously) according to the Law No. 19-12 of December 11, 2019, amending the territorial organization of the country, covering a total area of 2,150,900.00 ha (Programming and Budget Monitoring Department). Climatically, the study area enjoys a hot, dry, semi-arid environment with an average

rainfall of 124 mm/year and an average temperature exceeding 23°C.

Biskra has undergone an unprecedented urbanization trend in the past few decades. By 2018, the total population of Biskra Province was 930,580, of whom 569,013 (61,15%) were urban residents. In this study, we will exclusively target the Biskra urban area, which was designated in the 2016 Master Plan. The Biskra urban area covers a total of 44,600.00 ha and comrises three municipalities: Biskra (the capital city), Chetma, and El Hadjeb (Table 1).

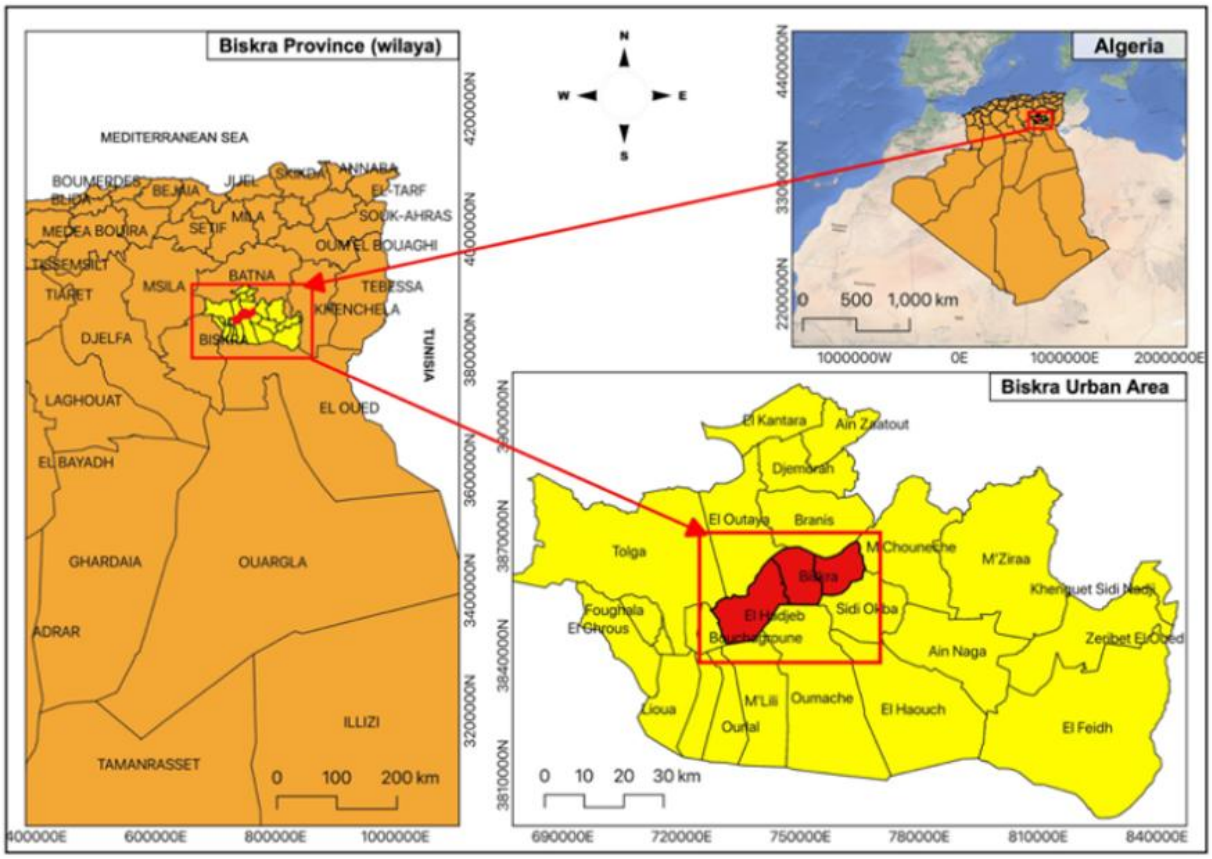

Figure 1. Case study location map
Source: Authors

Table 1. Biskra urban area statistics: Area and population

Municipalities	Area ha	Population (2000)	Population (2010)	Population (2020)
Biskra (capital city)	12,770.00	187,131	215,066	274,108
Chetma	11,020.00	8,807	14,380	17,522
El Hadjeb	20,810.00	8,989	10,591	13,500
Biskra urban area	44,600.00	204,927	240,037	305,130

Table 2. Landsat images characteristics

No.	Satellite	Sensor	Path/Row	Bands Used	Acquisition Date	Spatial Resolution (m)	Source
1	Landsat 7	ETM+	194/36	1, 2, 3, 4, 5 and 7	2000/09/22	30	USGS
2	Landsat 5	TM	194/36	1, 2, 3, 4, 5 and 7	2010/07/08	30	USGS
3	Landsat 8	OLI TIRS	194/36	1, 2, 3, 4, 5, 6 and 7	2020/07/19	30	USGS

3.2 Data

The data have been collected from several sources; three multispectral Landsat TM, ETM+, and OLI/TIRS satellite images were obtained from the United States Geological Survey (USGS) for the years 2000, 2010, and 2020 (Table 2). The demographic data was collected from the National Office of Statistics (ONS) and the Department of Programming and Budget Monitoring (DPSB). The master plans for 1998, 2008, and 2016 have been obtained from the Department of Urban Planning, Architecture and Construction (DUAC).

3.3 Data preparation and image pre-processing

To improve comparability across years, all images used in this work were collected during the same period (summer) under clear atmospheric conditions (cloud cover < 0.2%). The datasets were imported into QGIS 3.16 software for processing.

Geometrically, the Landsat imagery was rectified to the UTM projection method (datum WGS 84, Zone 31N). The study area has been extracted by clipping the raster using the georeferenced boundary outline of the Biskra urban area (shapefile). Subsequently, standard image pre-processing

operations were performed, including radiometric and atmospheric corrections using the Dark Object Subtraction 1 (DOS1) method. Georectification was implemented using a second-order polynomial and nearest-neighbor resampling technique. Furthermore, Digital Numbers (DN) of all the images were converted to Top of Atmosphere reflectance (TOA). The shadows in the Landsat images were detected, masked, and then filled using the method developed by Jin et al. [59].

3.4 Image classification

In this study, a supervised classification method based on a maximum likelihood algorithm was applied in QGIS 3.16 using the SCP plugin [60]. The first step consists of creating a false-color composite by combining three raster layers (bands) to serve as a background for selecting training samples (ROIs). Three major land use/cover classes have been identified in the study area: palm grove, bare soil, and built-up (Table 3).

Table 3. Descriptions of LULC classes

No.	LULC Class	Description
1	Built-up	Infrastructure (Settlements, commercial, industrial, Residential, transportation infrastructure, roads)
2	Palm grove	Palm grove and other types of agricultural practices (mostly palm trees)
3	Bare soil	Areas with almost no trees, exposed soil and flooded areas, bare rock areas

Training samples were generated as Regions of Interest (ROIs) using the SCP "ROI creation" dock. To capture the full spectral variability of each class, we utilized a combination of manual polygon digitization (for homogeneous areas) and a region-growing algorithm (for complex, heterogeneous features). The spectral signatures were inspected to ensure class separability before classification.

The sample size for training was determined using the Band Multiplier Rule (30n), specific to parametric classifiers such as the MLC Classifier, as recommended by Jensen [61]. This ensures sufficient degrees of freedom to estimate the class covariance matrices accurately, preventing matrix singularity in the classification process. Following the guidelines set forth by Jensen [61], an ideal sample size of 30n pixels per class was targeted, where n is the number of spectral bands used. As the classification used six spectral bands, the required minimum sample size per class was calculated as $30 \times 6 = 180$ pixels (540 pixels in total). For each of the three years (2000, 2010 and 2020), ROIs were digitized in QGIS using the SCP plugin, ensuring that each of the three land cover classes (Built-up, palm grove, and bare soil) contained at least 180 homogeneous pixels to satisfy the statistical requirements of the MLC.

Samples were spatially stratified across the entire extent of the satellite imagery to account for intra-class spectral diversity. Special care was taken to avoid spatial autocorrelation by ensuring training and validation polygons were geographically distinct.

Finally, supervised classification was performed using the MLC Classifier. MLC assumes that training data for each land-cover class follow a multivariate normal distribution. For each class, SCP computed the class mean vector and full covariance matrix. The discriminant function followed the standard Gaussian formulation, and pixels were assigned to the class with the highest posterior probability. Equal prior probabilities were used, and a probability threshold of 0.0001 was applied to reject low-confidence classifications. Complete methodology is outlined in Figure 2.

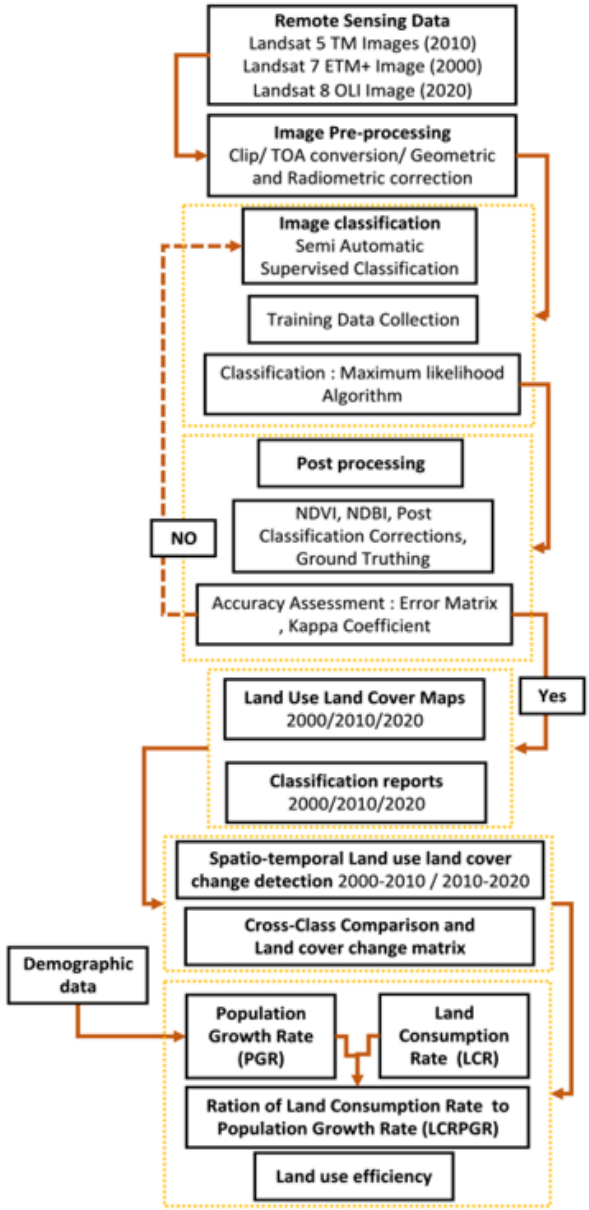

Figure 2. Research methodology flowchart

3.5 Spectral separability analysis

To produce the highest classification accuracy, it is essential to analyze the separability of the classes [62]. Therefore, we conducted a separability analysis of the three land cover classes identified in the study area. The spectral distance, or class separability, can be assessed using different distance measures.

In this study, we used the Jeffries-Matusita distance to analyze spectral separability between land cover classes. JM distance is a widely used measure of spectral separability in remote sensing applications [63]. JM distance values range from 0 when the signatures are similar (no separability) and 2 when the signatures are very distinct (completely separable) [64].

The pairwise-calculated JM separability of the selected training samples for the three images of the study area shows

that JM values are most consistent between palm grove and bare soil, and between palm grove and built-up, and least consistent between built-up and bare soil. The highest JM separability is found between palm grove and bare soil and between palm grove and built-up (1.999). The lowest JM separability is found between built-up and bare soil (1.91). Overall, the palm grove is the class that can be most easily separated from the other classes (High separability).

However, it is important to note that built-up overlaps heavily with bare soil; thus, they are relatively poorly separated and produce some misclassification in later steps. Post-classification refinements were used to reduce the observed misclassification.

3.6 Post-classification processing

Post-classification refinements were used to decrease the observed misclassification affected by the resemblances in spectral signatures of specific classes, namely built-up and bare soil. Classification errors were corrected using ground truthing.

To enhance classification accuracy, some spectral indices, such as the normalized difference built-up index (NDBI) [65], normalized difference vegetation index (NDVI) [66], and normalized difference bareness index (NDBaI) [67], were also created for post-classification refinement of the initially classified images. NDBI, NDVI, and NDBaI are calculated using Eqs. (1)-(3), respectively (Table 4).

$$\text{NDBI} = {(SWIR - NIR)}/{(SWIR + NIR)} \quad (1)$$

$$\text{NDVI} = {(NIR - RED)}/{(NIR + RED)} \quad (2)$$

$$\text{NDBaI} = {(SWIR - TIRS)}/{(SWIR + TIRS)} \quad (3)$$

where,

For Landsat 5 and 7: (RED = Band 3), (NIR = Band 4), (SWIR = Bands 5 and 7), (TIRS = Band 6).

For Landsat 8: (RED = Band 4), (NIR = Band 5), (SWIR = Bands 6 and 7), (TIRS = Band 10 and 11).

The post-classification refinement relied on a set of index-based rules combining NDVI, NDBI and NDBaI to standardize the assignment of land-cover classes (Table 5). Pixels were first evaluated for vegetation, which was retained where, NDVI was high (≥ 0.35) and both built-up and bare-soil signals were low (NDBI < 0.20 and NDBaI ≤ 0). Built-up areas were then identified as pixels with a strong built-up response (NDBI ≥ 0.20) but low vegetation and bareness (NDVI < 0.35 and NDBaI ≤ 0). Bare soil was assigned to pixels with a pronounced bareness signal (NDBaI > 0) and simultaneously low NDVI and NDBI. Finally, for each binary class mask, small misclassified patches were removed, and fragmented objects were regularized using simple morphological opening/closing with a 3 × 3 structuring element and a minimum mapping unit of 4-9 pixels, which reduced speckle and ensured more homogeneous class regions. A complete workflow schematic is provided in Figure 3.

The resulting maps were examined and analyzed to detect changes in land use and land cover in the Biskra urban area over the last 20 years.

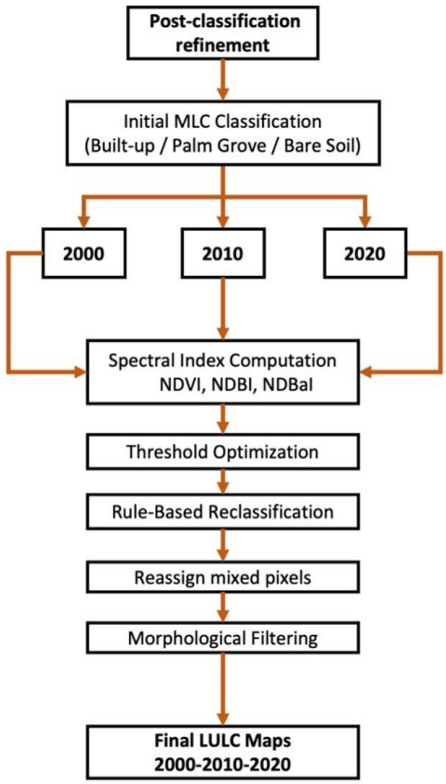

Figure 3. Post-classification refinement workflow

Table 4. Band mapping crosswalk for NDVI, NDBI and NDBaI

Index	Formulas	Band Used	TM 5	ETM+7	OLI 8
NDVI	(NIR-Red) / (NIR+Red)	NIR	Band 4	Band 4	Band 5
		Red	Band 3	Band 3	Band 4
NDBI	(SWIR-NIR) / (SWIR+NIR)	SWIR	Band 5	Band 5	Band 6
		NIR	Band 4	Band 4	Band 5
NDBaI	(SWIR-TIRS) / (SWIR+TIRS)	SWIR	Band 5	Band 5	Band 6
		TIRS	Band 6	Band 6	Band 10

3.7 Land use efficiency assessment using LCRPGR indicator

By definition, "Urban sprawl occurs when the growth rate of urbanized areas exceeds the population growth rate" [4]. To evaluate urban sprawl in a territory according to the EEA definition [4], it is necessary to calculate the ratio of land consumption to population growth. Therefore, UN-Habitat proposed an indicator to measure Land Use Efficiency (LUE) as a guideline for the Sustainable Development Goals (SDGs).

The indicator 11.3.1 (LCRPGR) measures the ratio of the rate at which urban land use expands against the population growth [68]. The two components of this indicator, Land Consumption Rate (LCR) and Population Growth Rate (PGR), are calculated using Eqs. (4), and (5), respectively:

$$\text{LCR} = {(V_{t1} - V_{t0})}/{V_{t0}} * {1}/{t} \quad (4)$$

where,

V_{t1} is the total built-up area in the current year

V_{t0} is the total built-up area in the past year

t is the number of years between V_{t1} and V_{t0}

Table 5. Index thresholds and reclassification rules

Class	Index Thresholds	Reclassification Rule (From Initial Map)	Morphological Refinement (Binary Mask)
Palm grove	NDVI ≥ 0.35; NDBI < 0.20; NDBaI ≤ 0.00	If initial label = Vegetation AND NDVI ≥ 0.35 AND NDBI < 0.20 AND NDBaI ≤ 0.00 ⇒ keep Vegetation; else relabel according to other rules.	3 × 3 opening to remove speckle, then remove patches < 4 pixels.
Built-up	NDBI ≥ 0.20; NDVI < 0.35; NDBaI ≤ 0.00	If initial label = Built-up OR (non-Vegetation pixel with NDBI ≥ 0.20 AND NDVI < 0.35 AND NDBaI ≤ 0.00) ⇒ set to Built-up.	3 × 3 closing to fill small gaps, then remove patches < 4 pixels.
Bare soil	NDBaI > 0.00; NDVI < 0.35; NDBI < 0.20	If pixel is not Vegetation or Built-up and NDBaI > 0.00 AND NDVI < 0.35 AND NDBI < 0.20 ⇒ set to Bare soil.	3 × 3 opening, then minimum mapping unit of 4-9 pixels.

$$\mathrm{PGR} = {}^{\ln(Pop_{t+n}/Pop_t)}/_{y} \quad (5)$$

where,

ln is the natural logarithm value

Pop_t is the total population within the urban area/city in the past/initial year

Pop_{t+n} is the total population within the urban area/city in the current/final year

y is the number of years between the two measurement periods

The ratio of land consumption rate to population growth rate (LCRPGR) is calculated using Eq. (6):

$$\mathrm{LCRPGR} = {}^{LCR}/_{PGR} \quad (6)$$

4. RESULTS AND DISCUSSION

4.1 Accuracy assessment

Classification accuracy assessment was performed for all output images to evaluate the extent of classification accuracy [69]. Validation sampling points were generated using a stratified sampling. An estimate of the validation sample size *n* with this sampling design is provided by Cochran [70] (Eq. (7)):

$$n \approx \left(\frac{\sum_i^M W_i S_i}{S(\hat{0})}\right)^2 \quad (7)$$

where, W_i is class *i* proportion of the mapped area, the standard deviation of the stratum $S_i = \sqrt{(U_i\ (1\text{-}U_i))}$ with U_i is class *i* target user accuracy. *M* is the number of LULC classes, and $S(\hat{O})$ is the standard deviation of the target overall accuracy. We set the target $S(\hat{O}) = 0.01$ and U_i between 70% and 85% for all classes. The resulting estimated sample sizes from Eq. (7) are $n = 605$, $n = 594$ and $n = 600$ for the years 2000, 2010, and 2020, respectively (Table 6). To calculate the validation samples for each class, a rough approximation is to take the mean of the equal distribution ($N_i = n/M$) and the weighted distribution ($n_i = n*W_i$), which is $n_i = (n/M+n*W_i)/2$. Table 7 shows the estimated sample allocation for each class.

Consequently, 1799 validation points were used for validating both mapping products; these were assessed and labelled on-screen using high-resolution imagery in Google Earth. Finally, we calculated the errors associated with 95% confidence interval (CI) for the accuracy measures and the estimated LULC areas, using their respective estimated variance equations, following the best practices outlined by Olofsson et al. [69]. These processes were calculated statistically using the area-based error matrix. of Olofsson et al. [69] where each element represents the estimated area proportion for each class (Table 8).

Table 6. Estimation of the sample size (*n*) of the validation

Class	Area %	W_i	S_i	W_i*S_i	$S(\hat{O})$	n
Built-up	3.37	0.033	0.3	0.010	0.01	
Palm grove	5.20	0.052	0.14	0.007	0.01	
Bare soil	91.43	0.914	0.25	0.229	0.01	
Total				0.246		605
Class	Area %	W_i	S_i	W_i*S_i	$S(\hat{O})$	n
Built-up	6.06	0.060	0.3	0.018	0.01	
Palm grove	8.45	0.084	0.14	0.012	0.01	
Bare soil	85.48	0.854	0.25	0.214	0.01	
Total				0.244		594
Class	Area %	W_i	S_i	W_i*S_i	$S(\hat{O})$	n
Built-up	8.92	0.089	0.3	0.027	0.01	
Palm grove	8.57	0.085	0.14	0.012	0.01	
Bare soil	82.49	0.824	0.25	0.206	0.01	
Total				0.245		600

Source: Authors

Table 7. Allocated samples for each class for the years 2000-2010-2020

2000			
Class	**Weighted**	**Equal**	**Mean**
Built-up	20	201	112
Palm grove	31	201	116
Bare soil	553	201	377
Total			605
2010			
Class	**Weighted**	**Equal**	**Mean**
Built-up	36	198	117
Palm grove	50	198	124
Bare soil	508	198	353
Total			594
2020			
Class	**Weighted**	**Equal**	**Mean**
Built-up	54	200	127
Palm grove	52	200	126
Bare soil	495	200	347
Total			600

The error matrix and accuracy report have been generated using the SCP's accuracy assessment utility. The report illustrates four different accuracy results: producer accuracy, user accuracy, overall accuracy and kappa hat index. In terms of both user and producer accuracies, the user accuracy (2000) exceeded 98% for all classes except the palm grove class, which was about 72%, while the 2010 map reached 87% for all classes. Similarly, the 2020 map exceeded 81% for all classes. In the same vein, producer accuracy across all years and classes topped 94%. Overall classification accuracy for all

years surpassed 97%. The Kappa coefficients for the 2000, 2010, and 2020 maps are 0.91, 0.94, and 0.91, respectively. The accuracy assessment results for each classified satellite image for 2000, 2010, and 2020 have been found satisfactory, as shown in Table 8.

Table 8. The error matrix for the years 2000, 2010 and 2020, populated with estimated proportion of area as recommended by good practice

2000					
Class	**Built-Up**	**Palm Grove**	**Bare Soil**	**Area**	**W*i***
Built-up	0.0331	0	0.00057	1,502.03	0.033677969
Palm grove	0.0019	0.0408	0.0092	2,319.77	0.052013037
Bare soil	0	0	0.9143	40,777.98	0.914308994
Total	0.0350	0.0408	0.9241	44,599.95	1
Area	1,561.95	1,821.69	41,216.13	44,599.95	
SE	0.0010	0.0020	0.0019		
SE area	43.31	88.83	83.80		
95% CI area	84.90	174.12	164.25		
Producer accuracy [%]	94.76	100	98.94		
User accuracy [%]	98.28	72.29	99.99		
Overall accuracy [%] = 98.81					
Kappa hat classification = 0.91					
2010					
Class	**Built-Up**	**Palm Grove**	**Bare Soil**	**Total**	**W*i***
Built-up	0.0579	0	0.0027	2,702.69	0.060595061
Palm grove	0	0.0748	0.0097	3,769.54	0.084514135
Bare soil	0	0	0.8549	38,130.25	0.854890804
Total	0.0579	0.0748	0.8674	44,599.86	1
Area	2,580.84	3,335.67	38,685.69	44,599.86	
SE	0.0003	0.0005	0.0005		
SE area	11.17	21.69	24.40		
95% CI area	21.90	42.51	47.82		
Producer accuracy [%]	100	100	98.57		
User accuracy [%]	95.46	87.45	100		
Overall accuracy [%] = 98.75					
Kappa hat classification = 0.94					
2020					
Class	**Built-Up**	**Palm Grove**	**Bare Soil**	**Area**	**W*i***
Built-up	0.0760	0	0.0133	3,983.15	0.089288917
Palm grove	0	0.0762	0.0096	3,826.76	0.085783175
Bare soil	0	0	0.8249	36,799.77	0.824927908
Total	0.0760	0.0762	0.8480	44,599.41	1
Area	3,389.4	3,398.85	37,821.42	44,599.41	
SE	0.0006	0.0008	0.0010		
SE area	26.70	35.85	44.70		
95% CI area	52.33	70.27	87.62		
Producer accuracy [%]	99.97	100	97.35		
User accuracy [%]	81.67	88.38	99.99		
Overall accuracy [%] = 97.70					
Kappa hat classification = 0.91					

4.2 Land use land cover change dynamics

A significant LULC transformation occurred across the three municipalities of the urban area due to the rapid pace of urbanization, particularly in the first decade (Figure 4). Extensive results are demonstrated in Table 9, including area-adjusted estimates with uncertainties (95% CI).

Between 2000 and 2010, the built-up area in Biskra municipality increased from 1,369.89 ha (10.72%) to 2,160.90 ha (16.92%) by 791.01 ha (+57.74%) and the palm grove from 837.99 ha (6.56%) to 1,034.19 ha (8.10%) by 196.20 ha (+23.41%). Whereas, the built-up area in Chetma municipality increased from 87.93 ha (0.80%) to 233.91 ha (2.12%), by 145.98 ha (+166.02%), and the palm grove from 396.01 ha (3.59%) to 632.79 ha (5.74%), by 236.78 ha (+59.79%). Similarly, in El Hadjeb municipality, the built-up area has increased from 104.13 ha (0.50%) to 186.03 ha (0.89%), by 81.90 ha (+78.65%), and the palm grove from 587.61 ha (2.82%) to 1668.69 ha (8.02%), by 1081.08 ha (+183.98%). The bare soil area exhibited a decreasing trend across all three municipalities.

Overall, the built-up area in Biskra urban area has been extensively increased from 1,561.95 ha (3.50%) to 2,580.84 ha (5.79%) by 1,018.89 ha (+65.23%) and the palm grove from 1,821.69 ha (4.08%) to 3,335.67 ha (7.48%) by 1,513.98 ha (+83.11%). In contrast, bare soil decreased from 41,216.13 ha (92.41%) to 38,685.69 ha (86.73%), by -2,530.44 ha (-6.14%).

The increasing trend sustained in the second decade from 2010 to 2020; nevertheless, the growth rate has significantly decelerated. Thus, the built-up area in Biskra municipality has extended to 2,735.10 ha (21.41%) by 574.20 ha (+26.57%). While the palm grove has decreased slightly to 921.87 ha (7.22%), by -112.32 ha (-10.86%). In Chetma municipality, the built-up area has expanded to 366.12 ha (3.32%), by 132.21 ha (+56.52%), and the palm grove to 720.27 ha (6.35%), by 87.48 ha (+13.82%). Similarly, in El Hadjeb

municipality the built-up area has increased to 288.18 ha (1.39%), by 102.15 ha (+54.91%), and palm grove to 1,756.71 ha (8.44%), by 88.02 ha (+5.27%).

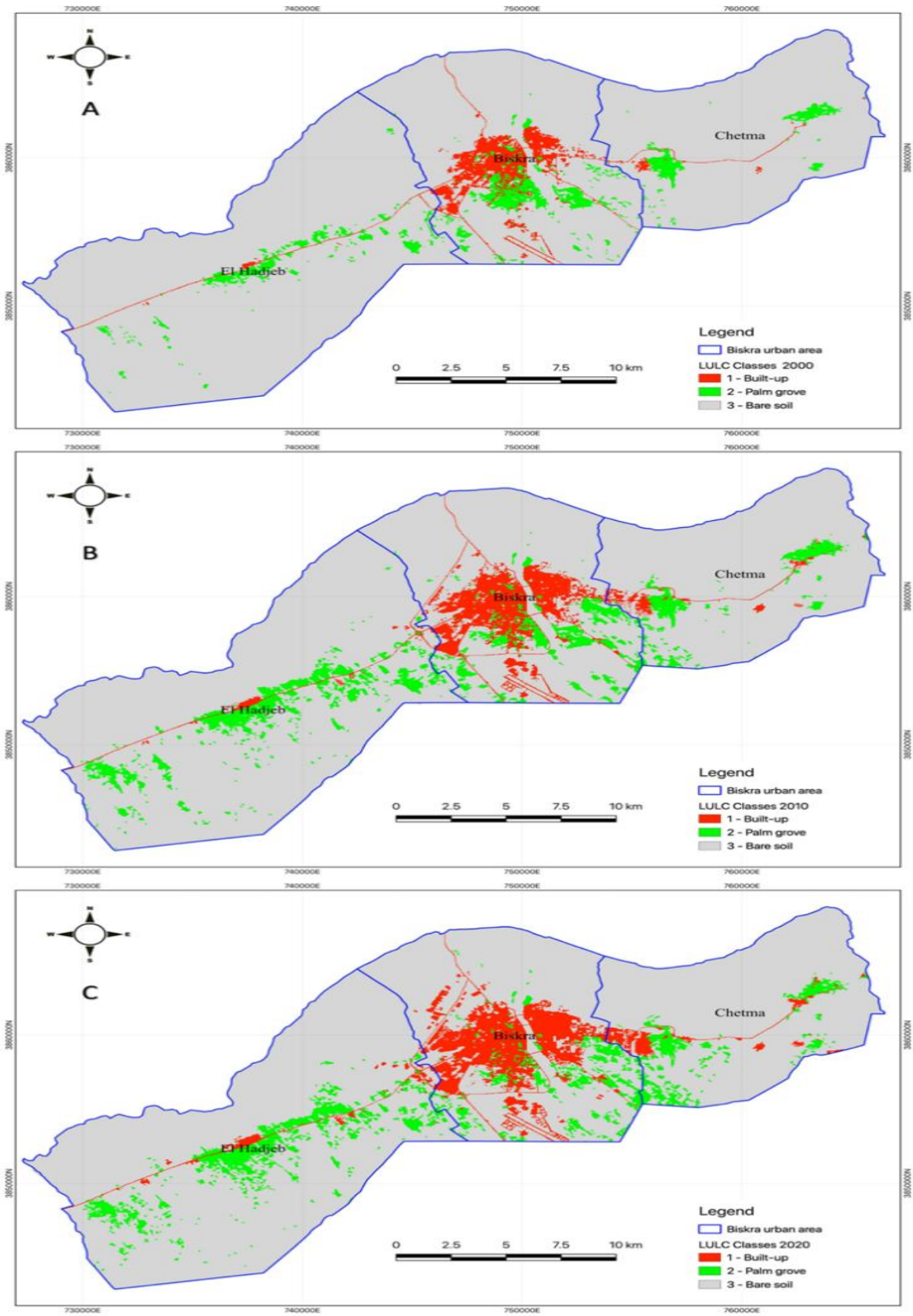

Figure 4. Classified LULC maps for the years (A) 2000, (B) 2010, and (C) 2020

Table 9. Area statistics (area-adjusted estimates with uncertainties 95%CI) for the years 2000, 2010 and 2020

Biskra Municipality											
	Percentage %			Area-Adjusted Estimates (ha)	95% CI (ha)	Area-Adjusted Estimates (ha)	95% CI (ha)	Area-Adjusted Estimates (ha)	95% CI (ha)	LULCC Change (ha)	
Class	2000	2010	2020	2000		2010		2020		2000/2010	2010/2020
Built-up	10.72	16.92	21.41	1,369.89	± 25.04	2160.9	± 7.51	2735.1	± 15.02	791.01	574.2
Palm grove	6.56	8.1	7.22	837.99	± 50.07	1034.19	± 10.01	921.87	± 20.03	196.2	-112.32
Bare soil	82.72	74.99	71.37	10,565.91	± 47.57	9578.7	± 12.52	911.82	± 25.04	-987.21	-461.88
Chetma Municipality											
	Percentage %			Area-Adjusted Estimates (ha)	95% CI (ha)	Area-Adjusted Estimates (ha)	95% CI (ha)	Area-Adjusted Estimates (ha)	95% CI (ha)	LULCC Change (ha)	
Class	2000	2010	2020	2000		2010		2020		2000/2010	2010/2020
Built-up	0.8	2.12	3.32	87.93	± 21.60	233.91	± 6.48	366.12	± 12.96	145.98	132.21
Palm grove	3.59	5.74	6.53	396.01	± 43.21	632.79	± 8.64	720.27	± 17.28	236.78	87.48
Bare soil	95.61	92.14	90.14	10,538.91	± 41.05	10,156.23	± 10.80	9,936.54	± 21.60	-382.68	-219.69
El Hadjeb Municipality											
	Percentage %			Area-Adjusted Estimates (ha)	95% CI (ha)	Area-Adjusted Estimates (ha)	95% CI (ha)	Area-Adjusted Estimates (ha)	95% CI (ha)	LULCC Change (ha)	
Class	2000	2010	2020	2000		2010		2020		2000/2010	2010/2020
Built-up	0.5	0.89	1.39	104.13	± 40.77	186.03	± 12.23	288.18	± 24.46	81.9	102.15
Palm grove	2.82	8.02	8.44	587.61	± 81.55	1,668.69	± 16.31	1756.71	± 32.62	1,081.08	88.02
Bare soil	96.67	91.08	90.17	20,111.31	± 77.47	18,948.51	± 20.39	18,758.34	± 40.77	-1,162.8	-190.17
Biskra Urban Area											
	Percentage %			Area-Adjusted Estimates (ha)	95% CI (ha)	Area-Adjusted Estimates (ha)	95% CI (ha)	Area-Adjusted Estimates (ha)	95% CI (ha)	LULCC Change (ha)	
Class	2000	2010	2020	2000		2010		2020		2000/2010	2010/2020
Built-up	3.50	5.79	7.60	1,561.95	± 84.90	2,580.84	± 21.90	3,389.4	± 52.33	1,018.89	808.56
Palm grove	4.08	7.48	7.62	1,821.69	± 174.12	3,335.67	± 42.51	3,398.85	± 70.27	1,513.98	63.18
Bare soil	92.41	86.73	84.78	41,216.13	± 164.25	38,685.69	± 47.82	37,821.42	± 87.62	-2,530.44	-864.27

Table 10. Cross-class comparison and LULC change matrix

Land Cover Change Matrix (ha) 2000-2010				
	> New Class 2010			
Reference Class 2000	Built-up	Palm Grove	Bare Soil	Total
Built-up	1,561.95	0	0	1,561.95
Palm grove	195.66	1,495.89	130.14	1,821.69
Bare soil	823.23	1,839.78	38,553.12	41,216.13
Total	2,580.84	3,335.67	38,685.69	44,599.77
Area change (ha)	1,018.89	1,513.98	-2,530.44	
Annual change rate (ha)	101.889	151.398	-253.044	
Land Cover Change Matrix (ha) 2010-2020				
	> New Class 2020			
Reference Class 2010	Built-up	Palm Grove	Bare Soil	Total
Built-up	2,580.84	0	0	2,580.84
Palm grove	63.27	2,524.5	747.9	3,335.67
Bare soil	745.92	874.26	37,063.71	38,685.69
Total	3,389.4	3,398.85	37,821.42	44,600.4
Area change (ha)	808.56	63.18	-864.27	
Annual change rate (ha)	80.856	6.318	-86.427	

Source: Authors

Table 11. Land-cover transition matrix for 2000-2010 and 2010-2020

Transition	2000-2010		2010-2020	
	Area (ha)	%	Area (ha)	%
Built-up to Palm grove	0	0	0	0
Built-up to Bare soil	0	0	0	0
Palm grove to Built-up	195.66	10.75	63.27	1.89
Bare soil to Built-up	823.23	2.06	745.92	1.96
Bare soil to Palm grove	1,839.78	4.75	874.26	2.31
Palm grove to Bare soil	130.14	7.06	747.9	22.69

Source: Authors

Conclusively, The Biskra urban area has experienced a similar increasing trend; thus, the built-up area has augmented to 3,389.40 ha (7.60%) by 808.56 ha (+31.33%), and the palm grove has slightly increased to 3,398.85ha (7.62%) by 63.18 ha (+1.89%). Conversely, bare soil has declined to 37,821.42 ha (84.78%) by -864.27 ha (-2.23%).

To better understand land encroachment across land classes over the past two decades, a change-detection matrix was prepared (Tables 10 and 11).

4.3 Cross-class comparison and LULC change detection matrix

A pixel-based comparison was employed to further explore the LULC change pattern using the SCP plugin. The change matrix was created by comparing image pairs of two different decades using cross-tabulation in order to evaluate quantitative and qualitative characteristics of LULC change as well as gains and losses in each class for the periods 2000 to 2010 and 2010 to 2020 (Table 10, Figure 5). Several critical change areas were identified after assessing and analyzing the amount, location, and nature of change in the study area.

Figure 4 shows that most of the change across all LULC classes and municipalities occurred in the first period, from 2000 to 2010 (Figure 5). During this period, the built-up area has gained 1,018.89 ha (+65.23%), with an annual growth rate of 101.88 ha/year (Table 10). 195.66 ha were transformed from palm groves (Table 11), located mainly to the south of Biskra Municipality (ancient town), a fact that can be explained by the properties' private nature.

Due to rising land values and growing demand, palm grove owners chose to convert their properties to urban land.

Conversely, in the second period from 2010 to 2020 (Figure 5), the growth rate has significantly declined. The built-up area has increased only by 808.56 ha (+31.33%), with an annual change rate of 80.85 ha/year, including 63.27 ha converted from palm grove (Table 11). This period was severely affected by the economic crisis (2008). Consequently, the majority of

construction projects, housing and urban development operations were cancelled.

Palm tree cultivation is the main agricultural activity in the Biskra urban area, particularly in the municipalities of Chetma and El Hadjeb. The livelihood of the majority of rural residents relies largely on it. Consequently, the percentage of palm groves has been gradually expanding from 2000 to 2020.

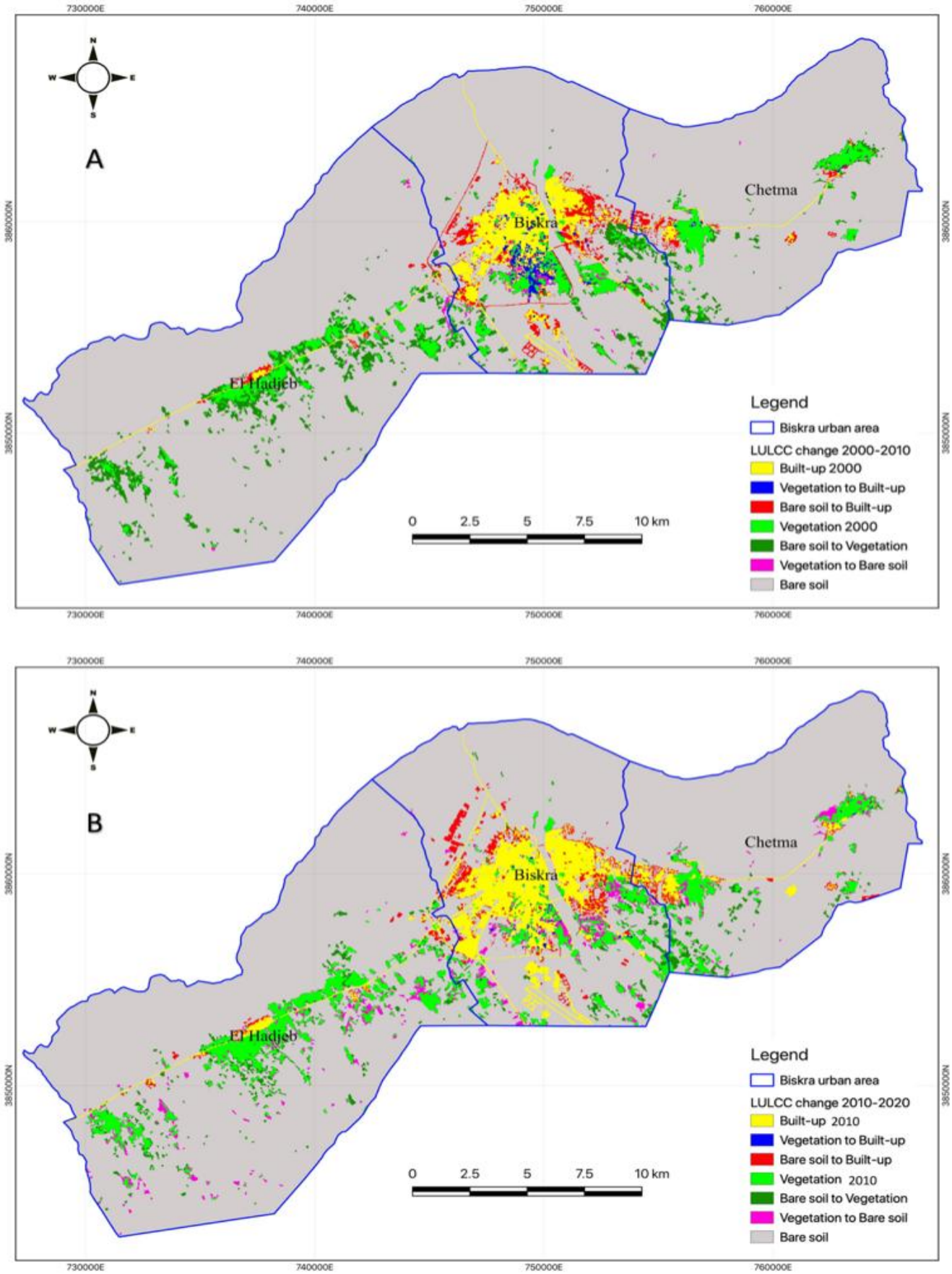

Figure 5. LULC change patterns, (A) 2000-2010 and (B) 2010-2020

The highest increase in the percentage of palm groves (and thus decreasing of bare soil) has been noticed between the years of 2000 and 2010 by 1,513.98 ha (+83.11%) mainly occurred in El Hadjeb by 1,081.08 ha (+183.98%) with an annual change rate of 151.39 ha/year (Table 10, Figure 5), which can be explained by the rise of small-scale farming following the inauguration of the agricultural support program by the Algerian government in 2000.

It is worth noting that despite the increase in the proportion of palm grove over the years, it lost 325.80 ha of its area between 2000 and 2010, including 195.66 ha converted to built-up area and 130.14 ha to bare soil (Table 11). On the other hand, from 2010 to 2020, the rate of growth of the palm grove area has sharply decreased from 83.11% to 1.89%, with an annual growth rate of 6.31 ha/year. Therefore, during this period, the palm grove has lost 811.17 ha (-24.31%) of its area, with 63.27 ha converted to built-up and 747.90 ha converted to bare soil (Table 11).

Spatially, these changes occurred at different locations, mainly in the south zone of Biskra (ancient town), along the RN 03, as well as on the eastern shore of Oued Biskra (Feliache agglomeration). Also, considerable change occurred in El Hadjeb toward RN 46. Furthermore, a substantial change was noticed to the east of Chetma municipality (Figure 5). The location of these changes can be explained by the influence of two driving forces: on one hand, the impact of main roads and on the other hand, the proximity to an urbanized area. These two factors increase land value, thereby encouraging palm grove owners seeking higher profits to convert their properties to urban land and prepare them for future urbanization.

Bare soil is the main land cover class in the study area. However, the results indicate a progressive decline in its proportion since it has been converted to other land use classes (Tables 10 and 11). During 2000-2010, a total of 823.23 ha was converted to built-up areas, and 1,839.78 ha was transformed into palm groves. Similarly, between 2010 and 2020, 745.92 ha were converted to built-up areas, and 874.26 ha to palm groves. The annual change rate was estimated at -253 ha/year (-6.14%) and -86.42 ha/year (-2.23%) during the periods 2000-2010 and 2010-2020, respectively (Table 10). The regression in bare soil area is principally attributed to the increasing rate of urbanization and the growing demand for cultivated land.

4.4 Urban sprawl, land use efficiency and sustainability

The results revealed that the Biskra urban area has evolved along several primary directions due to the influence of main roads, expanding further beyond the municipal boundary: eastward and westward (along RN 31 and RN 46), generating coalescence (conurbation) with Chetma and El Hadjeb, respectively. South-eastward (along RN 83) toward Feliache Agglomeration. Furthermore, toward the south (ancient town), where built-up areas are taking place on prime agricultural land and palm grove. Finally, and more recently, toward the north (along RN 03) (Figure 5).

The research indicated that, in addition to socio-economic drivers, land tenure (ownership) plays an important role in LULC change, as the majority of palm groves converted to built-up and bare soil were private properties. Therefore, landowners seeking higher profits are reluctant to contribute to palm grove conservation, leading to inappropriate land use and unsustainable land management practices that produce urban sprawl.

Furthermore, by comparing the Land Consumption Rate (LCR) with the Population Growth Rate (PGR), we assessed how efficiently the Biskra urban area utilizes land (Figure 6). The results obtained for the period 2000-2010 reveal that the LCR in Biskra, Chetma, El Hadjeb and overall Biskra urban area increased by 5.77%, 16.60%, 7.87% and 6.52% per year, respectively, while the PGR grew by 1.39%, 4.90%, 1.64% and 1.58% per year, respectively. The LCRPGR ratios obtained are clearly greater than one: 4.15, 3.39, 4.80, and 4.13, respectively (Figure 6), indicating that land consumption is growing four times faster than the population.

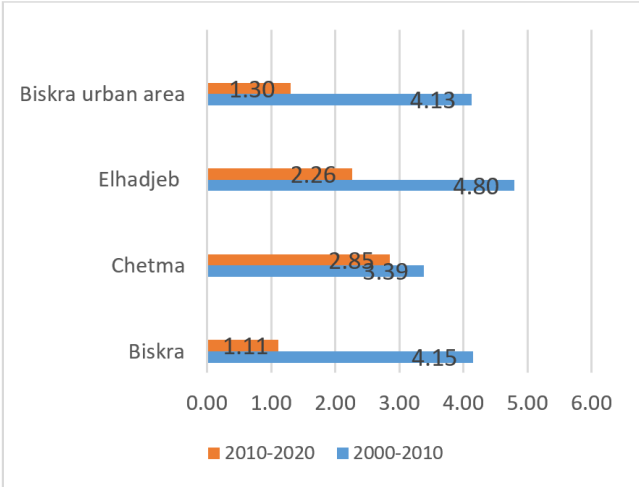

Figure 6. Ratio of land consumption rate to population growth rate (LCRPGR)

In 2010-2020, the ratios of LCRPGR obtained in Biskra, Chetma, El Hadjeb and overall Biskra urban area have considerably decreased to 1.11 (LCR = 2.66%, PGR = 2.4%), 2.85 (LCR = 5.65%, PGR = 1.98%), 2.26 (LCR = 5.49%, PGR = 2.43%) and 1.30 (LCR = 3.13%, PGR = 2.4%), respectively (Figure 5). Conclusively, the LCRPGR values imply that the Biskra urban area has experienced an uncontrolled urban sprawl mainly between 2000 and 2010, the sprawling trend sustained (LCPPGR > 1) between 2010 and 2020 with significant regression compared to the previous decade.

The results revealed the failure of current urban policies, land-use regulations, and master plans to monitor, control, and prevent urban sprawl. Hence, more sustainable land use policies are required.

4.5 Linking local urban sprawl dynamics to global trends

The urban expansion dynamics observed in the Biskra urban area closely reflect the global patterns identified by Seto et al. [8], particularly the systematic divergence between urban population growth and urban land consumption (Figure 6). Their global meta-analysis demonstrates that, across all regions, urban land expansion has consistently outpaced population growth, leading to declining LUE worldwide. The results obtained for Biskra clearly corroborate this trend. The calculated LCRPGR values remain persistently greater than one, especially after 2000, indicating that urban land expansion has progressed at a substantially faster rate than demographic growth (Figure 6). This confirms that the expansive growth pattern observed in Biskra is not exceptional but rather consistent with dominant global urbanization trajectories.

Seto et al. [8] further emphasized that, in developing regions, particularly in Africa, urban expansion is primarily driven by demographic growth rather than by economic performance alone. This interpretation aligns closely with the Biskra case, where rapid population growth and housing demand have been the principal drivers of spatial expansion, despite relatively moderate economic growth. The resulting urban form is characterized by outward expansion, reinforcing the global tendency toward inefficient land consumption documented by Seto et al. [8]. Spatially, the expansion in Biskra has followed principal transport axes and peri-urban fringes (Figure 5), illustrating the role of accessibility and infrastructure in shaping urban growth, as highlighted in the global literature.

Importantly, Seto et al. [8] note that a significant share of urban expansion cannot be fully explained by population and economic variables alone, underscoring the importance of local institutional and regulatory conditions. The findings from Biskra provide empirical support for this argument. Weak enforcement of planning regulations, fragmented land tenure, and the conversion of agricultural and oasis lands into urban plots have significantly facilitated uncontrolled expansion. These locally specific drivers correspond to the "unobserved factors" identified by Seto et al. [8] as critical determinants of urban growth outcomes. Consequently, the Biskra urban area case study not only confirms the global conclusions of Seto et al. [8] but also demonstrates how global urban expansion drivers are mediated through local socio-institutional dynamics in semi-arid cities.

5. CONCLUSIONS

The results show that the Biskra urban area experienced a massive, uncontrolled growth between 2000 and 2020. The study area witnessed aggressive urban sprawl, particularly in the first decade of the 21st century, as the built-up area grew four times faster than the population. Hence, the three distinct municipalities with distinct urban boundaries coalesced into a broad urban area where bare soils and palm groves were massively transformed into built-up areas to satisfy increasing housing and infrastructure demands.

Nevertheless, the urban sprawl trend of the 2000–2010 epoch has significantly decelerated in the last decade. This period was severely affected by the economic crisis (2008). Consequently, the majority of construction projects, housing and urban development operations were cancelled. Spatially, the built-up area stretched eastward and westward along the major roads linking the three municipalities (RN 31 and RN 46), extending beyond municipal boundaries. Moreover, the majority of the recently developed areas in the southern part of the study area (ancient town) are replacing palm groves that were once considered fertile and productive, creating a serious environmental issue.

Current urban policies have led to unsustainable, inefficient land management practices, resulting in a sprawled pattern of urbanization and significant land-use change. There is no evidence that this trend will change soon unless appropriate corrective actions are taken. From this perspective, local authorities and decision makers should devote more consideration to the issue of land use management and urban sprawl monitoring, starting with the implementation of an RS/GIS integrated approach to understand the past, present and future dynamics and trends of LULC change, to evaluate upcoming requirements, and to take actions to guarantee the suitability of future land supply.

GIS and remote sensing are powerful tools for monitoring and measuring urban sprawl. However, this study may have limitations in distinguishing built-up areas from bare land, which is among the most challenging tasks in land use land cover classification, particularly in arid and semi-arid contexts, as these regions have different spectral characteristics and a high degree of land homogeneity. Thus, more investigation into the application of different urban remote sensing indices is required.

ACKNOWLEDGMENT

We would like to thank USGS for its freely available Landsat imagery.

REFERENCES

[1] Seto, K.C., Sánchez-Rodríguez, R., Fragkias, M. (2010). The new geography of contemporary urbanization and the environment. Annual Review of Environment and Resources, 35(1): 167-194. https://doi.org/10.1146/annurev-environ-100809-125336

[2] Angel, S., Parent, J., Civco, D.L., Blei, A., Potere, D. (2011). The dimensions of global urban expansion: Estimates and projections for all countries, 2000-2050. Progress in Planning, 75(2): 53-107. https://doi.org/10.1016/j.progress.2011.04.001

[3] Friehat, T., Mulugeta, G., Gala, T.S. (2015). Modeling urban sprawls in northeastern Illinois. Journal of Geosciences and Geomatics, 3(5): 133-141. https://doi.org/10.12691/jgg-3-5-4

[4] EEA. (2006). Urban sprawl in Europe, the ignored challenge. https://doi.org/10.3280/asur2013-108001

[5] Ewing, R. (1997). Is Los Angeles-style sprawl desirable? Journal of The American Planning Association, 63(1): 107-126. https://doi.org/10.1080/01944369708975728

[6] Pendall, R. (1999). Do land-use controls cause sprawl? Environment and Planning B: Planning and Design, 26(4): 555-571. https://doi.org/10.1068/b260555

[7] Sudhira, H.S., Ramachandra, T.V., Jagadish, K.S. (2004). Urban sprawl: Metrics, dynamics and modelling using GIS. International Journal of Applied Earth Observation and Geoinformation, 5(1): 29-39. https://doi.org/10.1016/j.jag.2003.08.002

[8] Seto, K.C., Fragkias, M., Güneralp, B., Reilly, M.K. (2011). A meta-analysis of global urban land expansion. PLoS ONE, 6(8): e23777. https://doi.org/10.1371/journal.pone.0023777

[9] Al-sharif, A.A., Pradhan, B. (2014). Monitoring and predicting land use change in Tripoli Metropolitan City using an integrated Markov chain and cellular automata models in GIS. Arabian Journal of Geosciences, 7(10): 4291-4301. https://doi.org/10.1007/s12517-013-1119-7

[10] Al-Rashid, M.A., Nadeem, M., Aldosary, A.S., Harumain, Y.A.S., Arshad, H.S.H. (2021). An integrated approach to analysing the urban growth patterns: The case of Sialkot, Punjab, Pakistan. International Review for Spatial Planning and Sustainable Development, 9(4): 116-138. https://doi.org/10.14246/irspsd.9.4_116

[11] Martellozzo, F., Amato, F., Murgante, B., Clarke, K.C. (2018). Modelling the impact of urban growth on agriculture and natural land in Italy to 2030. Applied Geography, 91: 156-167. https://doi.org/10.1016/j.apgeog.2017.12.004
[12] Martellozzo, F., Ramankutty, N., Hall, R.J., Price, D.T., Purdy, B., Friedl, M.A. (2015). Urbanization and the loss of prime farmland: A case study in the Calgary-Edmonton corridor of Alberta. Regional Environmental Change, 15(5): 881-893. https://doi.org/10.1007/s10113-014-0658-0
[13] Grimm, N.B., Faeth, S.H., Golubiewski, N.E., Redman, C.L., Wu, J., Bai, X., Briggs, J.M. (2008). Global change and the ecology of cities. Science, 319(5864): 756-760. https://doi.org/10.1126/science.1150195
[14] Jat, M.K., Garg, P.K., Khare, D. (2008). Monitoring and modelling of urban sprawl using remote sensing and GIS techniques. International Journal of Applied Earth Observation and Geoinformation, 10(1): 26-43. https://doi.org/10.1016/j.jag.2007.04.002
[15] Yilmaz, M., Terzi, F. (2020). Characteristics of spatio-temporal urban growth patterns due to the driving forces of urbanization: The coastal city of Antalya, Turkey. International Review for Spatial Planning and Sustainable Development, 8(3): 16-33. https://doi.org/10.14246/irspsda.8.3_16
[16] Houet, T., Verburg, P.H., Loveland, T.R. (2010). Monitoring and modelling landscape dynamics. Landscape Ecology, 25(2): 163-167. https://doi.org/10.1007/s10980-009-9417-x
[17] Verburg, P.H., Van De Steeg, J., Veldkamp, A., Willemen, L. (2009). From land cover change to land function dynamics: A major challenge to improve land characterization. Journal of Environmental Management, 90(3): 1327-1335. https://doi.org/10.1016/j.jenvman.2008.08.005
[18] Ebraheem, A.K., Almosawi, F.M., Alkinani, A.S. (2024). The impact of unregulated urban sprawl on public services and quality of life in Baghdad: A case study of Al-Dora district using spatial analysis. International Journal of Sustainable Development & Planning, 19(12): 4715-4726. https://doi.org/10.18280/ijsdp.191218
[19] Mollah, T.H., Tahsin, M., Mohammad, N., Hasan, M.R., Mollah, N. (2020). Predicating land use / land cover changes for 2050 using CA- markov model and LCM: A case for Maheshkhali Island, Bangladesh. The Jahangirnagar Review, 44: 213-226.
[20] Rawat, J.S., Kumar, M. (2015). Monitoring land use/cover change using remote sensing and GIS techniques: A case study of Hawalbagh block, district Almora, Uttarakhand, India. The Egyptian Journal of Remote Sensing and Space Science, 18(1): 77-84. https://doi.org/10.1016/j.ejrs.2015.02.002
[21] Liping, C., Yujun, S., Saeed, S. (2018). Monitoring and predicting land use and land cover changes using remote sensing and GIS techniques-A case study of a hilly area, Jiangle, China. Westergaard-Nielsen A, editor. Plos One, 13(7): e0200493. https://doi.org/10.1371/journal.pone.0200493
[22] Ruiz-Luna, A., Berlanga-Robles, C.A. (2003). Land use, land cover changes and coastal lagoon surface reduction associated with urban growth in northwest Mexico. Landscape Ecology, 18(2): 159-171. https://doi.org/10.1023/A:1024461215456
[23] Indrayati, A., Rijanta, R., Muta'ali, L., Rachmawati, R. (2023). Built-up area changes, spatial pattern and urban sprawling in kedungsepur Metropolitan Area. International Journal of Sustainable Development & Planning, 18(8): 2541-2546. https://doi.org/10.18280/ijsdp.180825
[24] Epstein, J., Payne, K., Kramer, E. (2002). Techniques for mapping suburban sprawl. Photogrammetric Engineering and Remote Sensing, 68(9): 913-918.
[25] Lo, C.P., Choi, J. (2004). A hybrid approach to urban land use/cover mapping using Landsat 7 enhanced thematic mapper plus (ETM+) images. International Journal of Remote Sensing, 25(14): 2687-2700. https://doi.org/10.1080/01431160310001618428
[26] Aburas, M.M., Ho, Y.M., Pradhan, B., Salleh, A.H., Alazaiza, M.Y. (2021). Spatio-temporal simulation of future urban growth trends using an integrated CA-Markov model. Arabian Journal of Geosciences, 14(2): 131. https://doi.org/10.1007/s12517-021-06487-8
[27] Aplin, P. (2003). Comparison of simulated IKONOS and SPOT HRV imagery for classifying urban areas. In Remotely-Sensed Cities, pp. 23-46.
[28] Civco, D.L., Hurd, J.D., Wilson, E.H., Song, M., Zhang, Z. (2002). A Comparison of Land Use and Land Cover Change Detection Methods. Washington, D.C., USA.
[29] Shikary, C., Rudra, S. (2021). Measuring urban land use change and sprawl using geospatial techniques: A study on Purulia Municipality, West Bengal, India. Journal of the Indian Society of Remote Sensing, 49(2): 433-448. https://doi.org/10.1007/s12524-020-01212-6
[30] Chettry, V., Surawar, M. (2021). Urban sprawl assessment in eight mid-sized Indian cities using RS and GIS. Journal of the Indian Society of Remote Sensing, 49(11): 2721-2740. https://doi.org/10.1007/s12524-021-01420-8
[31] Bourenane, H., Bouhadad, Y. (2021). Impact of land use changes on landslides occurrence in urban area: The case of the Constantine City (NE Algeria). Geotechnical and Geological Engineering, 39(6): 1-21. https://doi.org/10.1007/s10706-021-01768-1
[32] Merghadi, A., Abderrahmane, B., Tien Bui, D. (2018). Landslide susceptibility assessment at Mila Basin (Algeria): A comparative assessment of prediction capability of advanced machine learning methods. ISPRS International Journal of Geo-Information, 7(7): 268. https://doi.org/10.3390/ijgi7070268
[33] Senouci, R., Taibi, N.E., Teodoro, A.C., Duarte, L., Mansour, H., Yahia Meddah, R. (2021). GIS-based expert knowledge for landslide susceptibility mapping (LSM): Case of mostaganem coast district, west of Algeria. Sustainability, 13(2): 630. https://doi.org/10.3390/su13020630
[34] Chen, D., Elhadj, A., Xu, H., Xu, X., Qiao, Z. (2020). A study on the relationship between land use change and water quality of the Mitidja watershed in Algeria based on GIS and RS. Sustainability, 12(9): 3510. https://doi.org/10.3390/su12093510
[35] Boudjemline, F., Semar, A. (2018). Assessment and mapping of desertification sensitivity with MEDALUS model and GIS-case study: Basin of Hodna, Algeria. Journal of Water and Land Development, 36(1): 17-26. https://doi.org/10.2478/jwld-2018-0002
[36] Azzouzi, S.A., Vidal-Pantaleoni, A., Bentounes, H.A.

(2017). Desertification monitoring in Biskra, Algeria, with Landsat imagery by means of supervised classification and change detection methods. IEEE Access, 5: 9065-9072. https://doi.org/10.1109/ACCESS.2017.2700405

[37] Afrasinei, G.M., Melis, M.T., Buttau, C., Bradd, J.M., Arras, C., Ghiglieri, G. (2017). Assessment of remote sensing-based classification methods for change detection of salt-affected areas (Biskra area, Algeria). Journal of Applied Remote Sensing, 11(1): 016025. https://doi.org/10.1117/1.JRS.11.016025

[38] Abdennour, M.A., Douaoui, A., Bennacer, A., Pulido Fernández, M., Bradai, A. (2019). Detection of soil salinity as a consequence of land cover changes at El Ghrous (Algeria) irrigated area using satellite images. Revue Agrobiologia, 9(1): 1458-1471.

[39] Dehni, A., Lounis, M. (2012). Remote sensing techniques for salt affected soil mapping: Application to the oran region of Algeria. Procedia Engineering, 33: 188-198. https://doi.org/10.1016/j.proeng.2012.01.1193

[40] Mendas, A., Delali, A. (2012). Integration of multicriteria decision analysis in GIS to develop land suitability for agriculture: Application to durum wheat cultivation in the region of Mleta in Algeria. Computers and Electronics in Agriculture, 83: 117-126. https://doi.org/10.1016/j.compag.2012.02.003

[41] Benaissa, F.T., Khalfallah, B. (2021). Industrial activity land suitability assessment using Delphi and AHP to control land consumption: The case study of bordj Bouarreridj, Algeria. Engineering, Technology & Applied Science Research, 11(5): 7738-7744. https://doi.org/10.48084/etasr.4362

[42] Hasbaia, M., Dougha, M., Benjedou, F. (2017). Erosion sensitivity mapping using a multi-criteria approach under GIS environment the case of the semiarid Hodna Basin in Central Algeria. International Journal of Water Resources and Arid Environments, 6(1): 13-19.

[43] Saadoud, D., Guettouche, M.S., Hassani, M., Peinado, F.J.M. (2017). Modelling wind-erosion risk in the Laghouat region (Algeria) using geomatics approach. Arabian Journal of Geosciences, Arabian Journal of Geosciences, 10(16): 363. https://doi.org/10.1007/s12517-017-3139-1

[44] Bensekhria, A., Bouhata, R. (2022). Assessment and mapping soil water erosion using RUSLE approach and GIS tools: Case of oued el-hai watershed, aurès west, northeastern of Algeria. ISPRS International Journal of Geo-Information, 11(2): 84. https://doi.org/10.3390/ijgi11020084

[45] Guettouche, M.S., Derias, A. (2013). Modelling of environment vulnerability to forests fires and assessment by GIS application on the forests of Djelfa (Algeria). Journal of Geographic Information System, 5(1): 24-32. https://doi.org/10.4236/jgis.2013.51003

[46] Benguerai, A., Benabdeli, K., Harizia, A. (2019). Forest fire risk assessment model using remote sensing and GIS techniques in Northwest Algeria. Acta Silvatica et Lignaria Hungarica: An International Journal in Forest, Wood and Environmental Sciences, 15(1): 9-21. https://doi.org/10.2478/aslh-2019-0001

[47] Rahmani, S., Benmassoud, H. (2020). Modeling and mapping forest fire risk in the region of Aures (Algeria). Geoadria, 24(2): 79-91. https://doi.org/10.15291/geoadria.2846

[48] Benameur, O., Leghrib, F., Laroui, A. (2024). Assessing urban green space accessibility for sustainable development in Mostaganem, Algeria: A space syntax approach. Journal of Contemporary Urban Affairs, 8(1): 197-211. https://doi.org/10.25034/ijcua.2024.v8n1-11

[49] Barbachea, A., Beghami, Y., Benmessaoudc, H. (2018). Study and diachronic analysis of forest cover changes of Belezma-Algeria. Geographica Pannonica, 22(4): 253-263. https://doi.org/10.5937/gp22-18806

[50] Sardou, M., Maouche, S., Missoum, H. (2016). Compilation of historical floods catalog of northwestern Algeria: First step towards an atlas of extreme floods. Arabian Journal of Geosciences, 9(6): 455. https://doi.org/10.1007/s12517-016-2490-y

[51] Abdelkebir, B., Maoui, A., Mokhtari, E., Engel, B., Chen, J., Aboelnour, M. (2021). Evaluating low-impact development practice performance to reduce runoff volume in an urban watershed in Algeria. Arabian Journal of Geosciences. Springer, 14(9): 814. https://doi.org/10.1007/s12517-021-07178-0

[52] Faregh, W., Benkhaled, A. (2021). GIS-based multicriteria approach for flood risk assessment in Sigus city, east Algeria. Arabian Journal of Geosciences, Arabian Journal of Geosciences, 14(12): 1152. https://doi.org/10.1007/s12517-021-07314-w

[53] Leghrib, F., Mazouz, S., Laroui, A., Benameur, O. (2021). Introducing urban growth models (UGM) in the algerian urban planning practice: Advantages and drawbacks. In Contemporary Approaches in Urbanism and Heritage Studies, pp. 119-130. https://doi.org/10.38027/N11ICCAUA2021272

[54] Bouhata, R., Kalla, M., Bensekhria, A., Habibi, Y. (2016). The spatio-temporal analysis of urban expansion of Biskra city (South Eastern Algeria) by the use of landsat satellite images. Annals of the University of Oradea, Geography Series/Analele Universitatii din Oradea, Seria Geografie, 26(2): 159-166.

[55] Adel, S., Hadda, D., Mahdi, K. (2018). Geomatics approach for urban extension management caught between planning tools and reality on the ground, case of the district of biskra (Algeria). Annals of the University of Oradea, Geography Series/Analele Universitatii din Oradea, Seria Geografie, 28(2): 156-163.

[56] Nedjai, R., Bensaid, A., Tuan, V.N., Haouchiche, A., Nasredine, M.N. (2016). Application of remote sensing and GIS to assess the construction pressure on the environment of Algiers (Algeria) during the three last decades and their evolution by the use of Markov Chain. Journal of Remote Sensing & GIS, 5(2.10000161). https://doi.org/10.4172/2469-4134.1000161

[57] Dechaicha, A., Daikh, A., Alkama, D. (2021). Monitoring and landscape quantification of uncontrolled urbanisation in oasis regions: The case of Adrar city in Algeria. Journal of Contemporary Urban Affairs, 5(2): 209-219. https://doi.org/10.25034/ijcua.2021.v5n2-5

[58] Dridi, H., Bendib, A., Kalla, M. (2015). Analysis of urban sprawl phenomenon in Batna city (Algeria) by remote sensing technique. Analele Universităţii din Oradea, Seria Geografie, 2: 211-220. https://doi.org/10.13140/RG.2.1.1128.0249

[59] Jin, S., Homer, C., Yang, L., Xian, G., Fry, J., Danielson, P., Townsend, P.A. (2013). Automated cloud and shadow detection and filling using two-date Landsat imagery in the USA. International Journal of Remote

Sensing, 34(5): 1540-1560. https://doi.org/10.1080/01431161.2012.720045
[60] Congedo, L. (2021). Semi-automatic classification plugin: A python tool for the download and processing of remote sensing images in QGIS. Journal of Open Source Software, 6(64): 3172. https://doi.org/10.21105/joss.03172
[61] Jensen, J.R. (2015). Introductory Digital Image Processing: A Remote Sensing Perspective. 4th Edition. Pearson Series in Geographic Information Science.
[62] Kulkarni, K., Vijaya, P.A. (2021). Separability analysis of the band combinations for land cover classification of satellite images. International Journal of Engineering Trends and Technology, 69(8): 138-144. https://doi.org/10.14445/22315381/IJETT-V69I8P217
[63] Padma, S., Sanjeevi, S. (2014). Jeffries Matusita based mixed-measure for improved spectral matching in hyperspectral image analysis. International Journal of Applied Earth Observation and Geoinformation, 32(1): 138-151. https://doi.org/10.1016/j.jag.2014.04.001
[64] Dabboor, M., Howell, S., Shokr, M., Yackel, J. (2014). The Jeffries-Matusita distance for the case of complex wishart distribution as a separability criterion for fully polarimetric SAR data. International Journal of Remote Sensing, 35(19): 6859-6873. https://doi.org/10.1080/01431161.2014.960614
[65] Zha, Y., Gao, J., Ni, S. (2003). Use of normalized difference built-up index in automatically mapping urban areas from TM imagery. International Journal of Remote Sensing, 24(3): 583-594. https://doi.org/10.1080/01431160304987
[66] Aburas, M.M., Abdullah, S.H., Ramli, M.F., Ash'aari, Z.H. (2015). Measuring land cover change in Seremban, Malaysia using NDVI index. Procedia Environmental Sciences, 30: 238-243. https://doi.org/10.1016/j.proenv.2015.10.043
[67] Zhao, H., Chen, X. (2005). Use of normalized difference bareness index in quickly mapping bare areas from TM/ETM+. International Geoscience and Remote Sensing Symposium, Seoul, 3: 1666. https://doi.org/10.1109/IGARSS.2005.1526319
[68] UN-Habitat. (2018). SDG indicator 11.3.1 training module: Land use efficiency. https://unhabitat.org/sites/default/files/2021/08/indicator_11.3.1_training_module_land_use_efficiency.pdf.
[69] Olofsson, P., Foody, G.M., Herold, M., Stehman, S.V., Woodcock, C.E., Wulder, M.A. (2014). Good practices for estimating area and assessing accuracy of land change. Remote Sensing of Environment, 148: 42-57. https://doi.org/10.1016/j.rse.2014.02.015
[70] Cochran, W.G. (1977). Sampling Techniques. John Wiley & Sons, New York. https://archive.org/details/samplingtechniqu0000coch_t4x6.

NOMENCLATURE

LULC	land use land cover
GIS	geographic information system
RS	remote sensing
SDGs	Sustainable Development Goals
LUE	land-use efficiency
EEA	European Environmental Agency
CBD	central business district
USI	urban sprawl index
TM	thematic mapper (landsat)
ETM+	enhanced thematic mapper (landsat)
OLI	operational land imager (landsat)
USGS	United States Geological Survey
DPSB	department of Programming and Budget Monitoring
DUAC	Department of Urban Planning, Architecture and Construction
ONS	national office of statistics
DOS1	dark object subtraction 1 method
DN	digital numbers
TOA	top of atmosphere reflectance
SCP	semi-automatic classification plugin
ROIs	regions of interest
JM	Jeffries-Matusita distance
NDBI	normalized difference built-up index
NDVI	normalized difference vegetation index
NDBaI	normalized difference bareness index
NIR	near-infra-red
SWIR	short wave infra-red
TIRS	thermal infra-red sensor
LCR	land consumption rate
PGR	population growth rate
LCRPGR	ratio of land consumption rate to population growth rate indicator
ha	hectare
RN	national road